

Supporting Information

Malinowski et al. 10.1073/pnas.1700762114

SI Materials and Methods

Planarian Maintenance. Specimens of clonal asexual *D. japonica* were used for all fission experiments. Planarians were stored in Tupperware containers in the dark in a temperature-controlled Panasonic incubator at 20 °C in planarian water (36) or instant ocean water (37). Planarians were fed organic beef or chicken liver from a local butcher three times a week to increase growth rates and the chance of fission (11). Worms were cleaned 2 h after feeding and starved for 1 wk before being used for experiments. Since planarians do not need a brain to fission, specimens were decapitated to increase the likelihood of fission in the presence of light (34). Cuts were performed with a clean razor blade perpendicular to the head–tail axis and as close to the head as possible. We did not detect any effects of the cuts on fission dynamics. Moreover, wound healing is quick (a few hours) compared with when fission first occurred, which was at least one but often several days after worms were amputated. Thus, planarians depicted in the movies, except for the weight experiments and Movie S1, do not have a head. Animals used for observation ranged between 0.5 and 1.2 cm in length after decapitation.

Fission Recording and Data Analysis. The substrate and planarians were imaged from 20 cm below with a FireWire A641f CCD camera (Basler AG) recording continuously at 0.8–3 frames per s (fps) using a custom-written MATLAB (MathWorks) script. The water was replaced completely and the gel surface washed at least once a week with planarian water. Planarians were exchanged either after successful fission or after 2 wk without reproducing. For each fission event, the corresponding image sequence showing only the animal engaged in fission was isolated and cropped using ImageJ (NIH). All image analysis was done using ImageJ or MATLAB. Worm areas, contact areas with the substrate (adhesion regions), and tail areas postpharynx were manually measured in ImageJ. Head and tail adhesion regions as well as their sum were found to scale linearly with worm size (Fig. S2). Linear fits of these measurements in MATLAB were then used to predict the total adhesion region size of a planarian based on its total size. The predicted sizes were then compared with the available tail areas postpharynx in individuals that divided prepharynx.

Kymograph and Fission Color Sequences. The kymograph shown in Fig. 3B was generated in ImageJ by plotting the pixel intensity of the red line shown in Fig. S3E for each image in the sequence and plotting lines for consecutive images from top to bottom. Sharp lines in kymographs correspond to moving sharp features (such as edges), and the slope of the line is proportional to the velocity of the feature. Artificial color sequences of fission events to emphasize body shape changes were obtained through inversion of the raw images, manual masking of the planarians at two consecutive time points, and subsequent subtraction of the resulting two images. The background is shown in white while colors correspond to differences in gray levels between the two time points. Positive differences correspond to gain of material while negative ones correspond to loss.

Single-Worm Statistical Data. Planarians were kept as individuals in separate Petri dishes, 100 mm in diameter and 20 mm in height (Fisher Scientific), containing 25 mL of planarian water. They were fed organic liver once per week, cleaned twice per week, and checked for divisions three times per week (7). Fissions were

tracked using the SAPling database and barcode system (35). Planarians were imaged at birth with a Leica S6D stereo microscope (Leica Microsystems) using a Basler A601f CCD camera equipped with Pylon viewer software (Basler AG). Planarian outlines were obtained using boundary detection in ImageJ and MATLAB. From these, the area at division was obtained by summing the areas of the head and tail offspring. The percentage of head at division was obtained by dividing the size of the head offspring at birth by the area at division of the parent worm. The pharynx position was measured as its relative position along the length of the worm either at birth or before division. Overall, our dataset represents 1,335 fission events with information on the worm identity at birth (head or tail), its ancestry, its area at birth and at division, and its RWT. Pharynx positions were only measured manually on a subset of these worms.

Through visual inspection we found that a cutoff at 56% of head at division binarized the data into pre- and postpharynx fission events. From this binarization we computed the fraction of prepharynx fissions as a function of RWTs.

Gel Preparation and Traction Force Measurements. Deformable gel substrates were prepared from CY 52-276 silicone gel (Dow Corning), by mixing the A and B components of the gel at a ratio of 1.2:1. The two components were thoroughly mixed in a 50-mL test tube over a period of 5 min using an overhead stirrer. The mixture was then degassed by centrifuging the test tube at $\sim 400 \times g$ for 3 min. The gel prepolymer was poured into 60-mm Petri dishes to form ~ 5 -mm layers which were baked for 15 min on a 95 °C hot plate to initiate cross-linking of the gel, making it sufficiently solid to withstand spin coating with a thin layer of the gel prepolymer. As the Petri dishes baked, glass tracer particles (30- to 45- μm glass beads, purchased from Amazon as “Green Glow in the Dark Pigment Powder”) were mixed with an aliquot of the gel prepolymer at a mass ratio of 1:12. The suspension of the bead in the prepolymer was deposited onto surfaces of the prebaked gel in the 60-mm Petri dishes and the dishes were spun on a spin coater at 1,200 rpm for 20 s, producing ~ 70 - μm -thick layers of the bead suspension. Finally, the Petri dishes were covered, flipped upside down to make the beads move toward the gel surface, and baked overnight in an 80 °C oven. The Young’s modulus of the silicone gel was measured at 1.2 kPa using a recently developed gel rheometer (38). The substrate and planarians were imaged using the same method described above. The observed bead motion was measured using custom-written scripts in MATLAB and converted into traction stresses using the scripts previously published and distributed in ref. 24.

Planarian Pulling. Worms in planarian water were subjected to external stresses using a peristaltic pump (Cole Parmer). The inlet was split forked into two and capped with nested plastic pipette tips (TipOne; USA Scientific) to decrease the cross-sectional area over which the force by the pump was being applied. The inner diameter of the pipette tip (P10) was 0.48 mm and chosen empirically to allow for an individual planarian, comparable in size to the specimen used in fission experiments, to be sucked a considerable amount into the pipette tip.

The tips were positioned at the anterior and posterior ends of the planarian, and the pump’s revolutions per minute (rpm) were slowly increased until the worm was ripped apart. The rpm necessary to rip a planarian varied little between individuals. Pulling experiments were imaged from above using a Leica S6D Stereo Microscope and a Basler A611f CCD camera with Pylon

viewer software. Upper and lower bounds for the stress applied to the planarian were calculated using the peristaltic pump to lift chrome steel beads. The pump was able to lift $n = 5$ beads of mass $6.26 \pm 0.01 \times 10^{-5}$ kg at the rpm necessary to rip a planarian, giving us a lower bound for the applied stress, and was unable to lift $n = 5$ beads of mass $1.31 \pm 0.01 \times 10^{-4}$ kg at the rpm necessary to rip a planarian, giving us an upper bound for the applied stress. The beads that were tested were of masses $5.25 \pm 0.01 \times 10^{-5}$ kg, $6.26 \pm 0.01 \times 10^{-5}$ kg, $1.31 \pm 0.01 \times 10^{-4}$ kg, $2.57 \pm 0.01 \times 10^{-4}$ kg, $4.34 \pm 0.01 \times 10^{-5}$ kg, and $4.43 \pm 0.01 \times 10^{-4}$ kg, giving us a range of 3.9×10^{-4} kg. Only the $5.25 \pm 0.01 \times 10^{-5}$ kg and $6.26 \pm 0.01 \times 10^{-5}$ kg masses could be lifted at rpm necessary to rip a planarian. The stress was calculated using Newton's second law on the bead, $pA = g(m_{\text{bead}} - \rho_{\text{water}} \frac{4}{3}\pi r^3)$, where p is the pressure of the pump, A is the cross-sectional area of the pipette tip, m_{bead} is the mass of the bead, g is gravitational acceleration, ρ_{water} is the density of water, and r is the radius of the bead. This yielded a lower-bound stress of 7.0 kPa and an upper-bound stress of 13.1 kPa.

Mucus Pulling Experiments. Experiments were performed using a horizontally mounted Leica stereo S8APO microscope, equipped with a Point Gray Flea USB 3 camera (Point Gray) mounted on a ring stand (Fisher Scientific). Image sequences were captured using a custom MATLAB script. Backlighting was provided using a G-2001 cold LED panel (GEPE). To generate mucus, planarians were cut on a clean glass slide (Fisher Scientific). The slide was then mounted on a glass panel for imaging. An M-152 micromanipulator (Narshige) with a 200- μ L pipette tip (Fisher Scientific) attached to the end was moved into the mucus until some mucus got stuck to its tip. Video recording was started and the tip was lifted until the mucus film was stretched to its maximum length and ruptured. Mucus lengths were obtained in ImageJ and MATLAB by measuring length of mucus in the last frame before rupture occurred.

Planarian Crushing. For top-view movies, a 5-g weight (Troemner) was put onto the tail region of a planarian and the worm was imaged using a Leica S6D stereo microscope and a Basler A601f CCD camera with Pylon viewer software. For side-view and bottom-view movies, the same 5-g weight was put onto the tail region of the planarian and imaged using a Leica stereo S8APO microscope and a Point-Gray camera controlled by MATLAB. Images were analyzed using ImageJ and MATLAB and head length was measured as defined in Fig. S8.

Planarian Density. To determine an approximate value for the typical density of *D. japonica*, 10 planarians were imaged individually from above using the Leica S6D stereo microscope and a Basler A601f CCD camera with Pylon viewer software. The worms were then weighed all together on an AE 200 (Mettler Toledo) scale. To calculate the density, the total mass recorded was then divided by the total volume of the worms, which was estimated by assuming the worm was an ellipsoid. The worm length and width were measured from the top-view images in ImageJ, and the worm height was assumed to scale with worm width as shown in ref. 36.

Antibody Staining. Asexual *Schmidtea mediterranea* planarians were used for antibody staining because of their smaller size at fission (7). Antibody staining was performed using standard protocols (39). For nervous system staining, randomly selected *S. mediterranea* were used. *S. mediterranea* observed to undergo waister formation in preparation of fission were fixed before rupture for the muscle staining experiments. Since fission cannot be controlled, it was unknown at which state during fission fixation was performed. Specimens were fixed in 4% paraformaldehyde in $1 \times$ PBS for 20 min and bleached overnight in 100% methanol supplemented with 6% hydrogen peroxide. They were incubated

overnight at 4 °C with either an antimuscle or antisynapsin antibody raised in mouse from the Developmental Studies Hybridoma Bank (clone 6G10-C7 for antimuscle and clone 3C11 for antisynapsin) diluted 1:500 in antibody blocking buffer consisting of PBS supplemented with 0.3% Triton-X (Sigma Scientific), 0.1% Tween-20 (Sigma Scientific), 1% FBS (Sigma Scientific), and 0.1% DMSO (Sigma Scientific). After 4–6 h of washes, worms were incubated overnight at 4 °C with an Alexa488-conjugated anti-mouse secondary antibody (Thermo Fisher) diluted 1:500 in antibody blocking buffer. Specimens were imaged using an inverted IX81 spinning disk confocal microscope (Olympus Corporation) controlled by Slidebook software (Intelligent Imaging Innovations).

Mucus Rheology Measurements. Mucus was scraped off of planarians by repeatedly stroking them on their dorsal side with a soft plastic pipette tip. Mucus rheology was measured by placing the fresh mucus sample into an Anton Paar MCR301 rotational rheometer (Anton Paar) with a plate diameter of 2.5 cm and a gap width of 50 μ m between plates. Measurements of shear stress were made in response to oscillatory deformations with equally logarithmically spaced frequencies from 0.02 Hz to 9 Hz (Fig. S5). From shear stress τ , and shear deformation γ , the complex viscosity η was computed using $\eta = \tau / \gamma 2\pi f$. During fission, the “oscillatory stimulus” is the contraction phase of pulsation, which happens at about 0.023 Hz, so the mucus viscosity during fission is about 65 Pa-s.

Stickiness Experiments and Mucus Visualization. To determine the substrate adhesion (“stickiness”) of planarians, we placed individual *D. japonica* planarians into a 3D-printed plastic arena (150 mm \times 100 mm \times 16 mm), filled with 30 mL of ionized (IO) water, and allowed it to acclimate. The arena was printed using white PLA filament (MatterHackers) on a LulzBot Taz 6 (LulzBot). A water flow was briefly introduced to the planarian from a distance of ~ 25 mm. The flow rate was increased in discrete steps until the planarian was fully displaced. The flow was sourced by a 3D-printed reservoir (82.5 mm \times 82.5 mm \times 35 mm) attached to 5-mm-diameter silicon tubing, which was clamped onto a custom-built system with an automated variable-height shaft. Flow measurements were made with an Arduino UNO board (Arduino) and a Hall sensor (Amazon), connected in series with the tubing. Flow rate was controlled by varying the height difference between the reservoir and the arena. Each worm was measured twice. The initial experiment was conducted in IO water, then the planarian was incubated and allowed to rest for 1 min in either IO water or in IO water supplemented with detergent (0.02% Triton X-100). After incubation the same worm was measured again in IO water. Of note, measurements of untreated and treated worms were alternated and we did not observe any trends in stickiness over time. We report the relative stickiness as the ratio of the second measurement to the first one. To visualize mucus secretion induced by detergent exposure, planarians were treated with 0.025% Triton X-100 for 10 min. The longer incubation time was chosen to ensure that gliding trails could be visualized (16). For mucus staining, they were allowed to move on no. 1 coverslips. The staining was performed with fluorescein-conjugated VVA lectin as previously reported (16). Images were acquired on an Olympus IX81 inverted microscope. To visualize mucus trails, the exposure time had to be 2.5 times longer for control worms than for Triton X-100-treated planarians. In addition, image treatment was necessary to enhance contrast. Both demonstrate the larger amount of mucus secreted after treatment with Triton X-100.

SI Text

Morphometric Relationships in the Waist. We found that that the waist diameter is anatomically constrained and that it scales with

the initial width of the worm. One possibility is that actin fibers forming the circular muscles that contract during waist formation possess a nonlinear force–elongation relationship, as observed in the medicinal leech (40). The force required to contract the worm width by >70% (Fig. S4B) could be too large because of this nonlinearity. In addition, contraction of the circular muscles forces the longitudinal fibers closer together. It is conceivable that, at some degree of contraction, these fibers start resisting further compression and thus further reduction of diameter of the waist.

To understand what sets the ratio of head and waist cross-sectional areas and thus determines the amplification factor of stresses in the waist region, we measured total body length, total body width, waist length, waist width, head piece length, head piece width, tail piece length, and tail piece width of the 22 recorded fission events. We refer to these quantities as L_0 , B_0 , L_W , B_W , L_H , B_H , L_T , and B_T , respectively. We use B to denote width to avoid notation confusion between width and waist.

We found that L_W and B_W at the moment of rupture scaled linearly with, respectively, L_0 and B_0 (Fig. S4A and B) (i.e., longer, wider worms also form longer and wider waists) (see main text).

Furthermore, we observed that L_0 does not change during the formation of the waist, and thus

$$L_0 = L_H + L_W + L_T.$$

Because the head and tail pieces expand radially by the same factor relative to W_0 (Fig. S3C) and B_W scales linearly with B_0 , we can define two constants:

$$\alpha = \frac{B_H}{B_0} = \frac{B_T}{B_0}$$

$$\beta = \frac{B_W}{B_0}.$$

Combined with the incompressibility condition

$$L_0 B_0^2 = L_H B_H^2 + L_W B_W^2 + L_T W_T^2$$

these constraints imply that the ratio of L_W to L_0 is set by

$$\frac{L_W}{L_0} = \frac{1 - \alpha^2}{\beta^2 - \alpha^2}.$$

Inserting the experimental values of α and β from Fig. S4B and C sets the waist length to be a factor 0.263 times the original length, which agrees with the data in Fig. S4A.

Finally, since we also observed that L_0 and B_0 scale linearly (Fig. S4D), it logically follows that L_W and B_W also scale together, as shown in Fig. S4E.

Planarian Crushing Experiments. Because fission events are rare and cannot be induced on command, it is experimentally difficult to capture events at high spatial and temporal resolution. Therefore, we tried to mimic fission by pinning the tail region of a planarian down using a small weight and recording how it broke free. Although this scenario is not similar to fission biologically, it does provide additional insight into different aspects of fission dynamics at high spatial and temporal resolution. The weight experiments helped confirm that the planarian lifts its head during the pulsing phase. Side-view imaging allowed us to quantify the angle and the height at which the head is lifted (Fig. S6 and Movie S7). The height of head lifting is about 1 mm, consistent with our mucus pulling measurements, in which

we were able to stretch planarian mucus to a length of about 1 mm before breakage (Fig. S5). We thus conclude that the worm lifts its head to break free from the mucus to minimize drag during head extension.

In agreement with this picture, head elongation in the weight experiments followed the same logistic time course observed in fission, albeit at a significantly faster pace (Fig. S6). In this situation, we rarely observed multiple pulses, which is likely due to the fact that the worms were able to partially pull themselves out from underneath the weight before tearing. Occasionally, a narrowing would be visible close to the edge of the weight, vaguely resembling a waist region. However, the worm was always crushed by the weight and did not fission. Overall, these experiments demonstrate that head lifting during extensions is a key component of the fission process and is presumably used to reduce frictional drag and thus achieve higher strains for a given stress.

Model of Fission Dynamics. The dynamics of fission and its different steps poses questions as to the elastodynamics of planarians. Specifically,

- i) What are the physical ingredients controlling flesh waves/pulsations? Can the space–time response be calculated and/or characterized?
- ii) What determines the planarian’s relaxation time, after pulsation?
- iii) Can the radial impulse observed experimentally be shown to be consistent with the axial stresses in the waist when fission occurs?

To answer these questions, we use a linear approximation for tractability and model the worm (anterior) as a uniform, thin, cylindrical, elastic shell. The thin elastic shell model is justified by the anatomy of the worm, which can be coarse-grained into bulk material of density ρ encompassed by a muscle network of thickness h (Fig. S1). Our model assumes that the stiffness is set by the muscle network/shell rather than the worm’s interior (i.e., that the elastic modulus of the shell is significantly higher than that of the mesenchymal tissue). We use an experimentally estimated mean value for ρ since $\rho(r)$ is not available. Consistent with this approach, geometric nonlinearities are not treated.

The constitutive equations for such a thin shell using Donnell’s linear theory are (41)

$$\frac{\partial^2 u}{\partial z^2} + \frac{(1-\nu)}{2R^2} \frac{\partial^2 u}{\partial \varphi^2} + \frac{(1+\nu)}{2R} \frac{\partial^2 v}{\partial z \partial \varphi} + \frac{\nu}{R} \frac{\partial w}{\partial z} = \frac{1}{c_s^2} \frac{\partial^2 u}{\partial t^2} \quad [S1]$$

$$\frac{(1+\nu)}{2R} \frac{\partial^2 u}{\partial z \partial \varphi} + \frac{(1-\nu)}{2} \frac{\partial^2 v}{\partial z^2} + \frac{1}{R^2} \frac{\partial^2 v}{\partial \varphi^2} + \frac{1}{R^2} \frac{\partial w}{\partial \varphi} = \frac{1}{c_s^2} \frac{\partial^2 v}{\partial t^2} \quad [S2]$$

$$\frac{\nu}{R} \frac{\partial u}{\partial z} + \frac{1}{R^2} \frac{\partial v}{\partial \varphi} + \frac{w}{R^2} + \beta^2 \left(R^2 \frac{\partial^4 w}{\partial z^4} + 2 \frac{\partial^4 w}{\partial z^2 \partial \varphi^2} + \frac{1}{R^2} \frac{\partial^4 w}{\partial \varphi^4} \right) - \frac{p_a(1-\nu^2)}{Eh} = -\frac{1}{c_s^2} \frac{\partial^2 w}{\partial t^2}. \quad [S3]$$

Here u , v , and w refer to longitudinal (i.e., axial), azimuthal, and radial (flexural) perturbations of the shell (Fig. S1), R is the radius of the head, ν is the Poisson ratio, β is given by $h^2/12R^2$, p_a is the pressure, and c_s is the speed of sound $\sqrt{E/\rho}$, where E is the Young’s modulus of the worm and ρ is the mean density of the worm. The basic waves are coupled by finite Poisson ratio.

We then make assumptions that simplify these equations. First, azimuthal perturbations are ignored, as there is no evidence for

the role of twisting in fission dynamics. Second, loading is ignored ($p_a = 0$) because the planarian shell is—in contrast to nematodes (42)—not pressurized. In addition, acoustic coupling is irrelevant, that is, effective speeds are strongly subsonic as the speed of sound in the worm is 0.7 m/s and worm density is similar to that of water (*SI Materials and Methods*). Under these assumptions, the model supports two types of linear responses (and waves) corresponding to flexural and longitudinal perturbations, captured by the following simplified equations:

$$\frac{w}{R^2} + \beta^2 R^2 \frac{\partial^4 w}{\partial z^4} = -\frac{1}{c_s^2} \frac{\partial^2 w}{\partial t^2} \text{ flexural}$$

$$\frac{\partial^2 u}{\partial z^2} = \frac{1}{c_s^2} \frac{\partial^2 u}{\partial t^2} \text{ longitudinal.}$$

By assuming a wave solution to these equations of the form $e^{i(k_z z - \omega t)}$ we can derive the dispersion relation for these traveling waves.

Pure radial bending (i.e., flexural) waves have a dispersion relation $\omega_f^2 = c_s^2/R^2(1 + \beta^2 R^4 k_z^4)$, where k_z is the axial wave-number. The shell curvature ensures that the wave frequency exceeds the dissipative damping rate for the worm.

Pure longitudinal waves have $\omega_f^2 = k_z^2 c_s^2$. As pulsations are dominantly radial, the characteristic velocity of an initially localized pulse is set by the flexural wave group velocity, which can be calculated as

$$d\omega_f/dk_z = 2 \frac{c_s}{R} \frac{(\beta^2 R^4 k_z^3)}{(1 + \beta^2 R^4 k_z^4)^{1/2}}.$$

Taking $k_z \sim 2\pi/R$ yields a pulse velocity $v_{gw} = 1.4$ mm/s, which agrees well with the observed pulse velocity of 1.1 mm/s (Table S1). Since the response to pulsation is an axially propagating radial perturbation, the local treatment given here is consistent with experimental observations.

Using the same model assumptions, we then ask whether we can reproduce the time scale of length relaxation during pulsation. Slippage is determined by the competition between the axial elastic restoring force on the worm and friction of the worm with its substrate. We calculate the time scale for contraction using Newton's second law on the head piece with mass M_{head} . Thus, for axial displacement δz , we have

$$M_{\text{head}} \frac{d^2 \delta z}{dt^2} = -k_{\text{eff}} \delta z - \alpha \frac{d}{dt} \delta z, \quad \text{[S4]}$$

where $k_{\text{eff}} \delta z$ is the elastic longitudinal restoring force with an effective spring constant $k_{\text{eff}} = EV_{\text{head}}/L_{\text{head}}^2$, with E the Young's modulus, L_{head} the length of the head, and V_{head} the volume of the head. The form of k_{eff} follows from the axial restoring force one gets by linear longitudinal elastic forces. The friction coefficient α is set by viscous drag on the mucus layer. F_f , the friction force, is given by $F_f = -\eta_{\text{mucus}} A_c \partial v_z / \partial x$, where η_{mucus} is the mucus viscosity, A_c is the area of contact of the worm with the substrate, x is the depth in the mucus layer, and h_{mucus} is the thickness of the mucus layer. Taking $\partial v_z / \partial x \equiv v/h_{\text{mucus}}$ yields $F_f = -\eta_{\text{mucus}} A_c / h_{\text{mucus}} d/dt \delta z$.

We can substitute this into Eq. S4 and get

$$M_{\text{head}} \frac{d^2 \delta z}{dt^2} = -\frac{EV_{\text{head}}}{L_{\text{head}}^2} \delta z - \frac{\eta_{\text{mucus}} A_c}{h_{\text{mucus}}} \frac{d}{dt} \delta z.$$

As slip times are long compared with longitudinal inertial time scales, inertia is neglected ($M_{\text{head}} d^2 \delta z / dt^2 = 0$), so frictional drag balances axial forces and we can write

$$\eta_{\text{mucus}} \frac{A_c}{h_{\text{mucus}}} \frac{d}{dt} \delta z \equiv -\frac{EV_{\text{head}}}{L_{\text{head}}^2} \delta z$$

and obtain $1/\tau_{\text{slip}} \equiv V_{\text{head}} E h_{\text{mucus}} / L_{\text{head}}^2 \eta_{\text{mucus}} A_c$ for the inverse slip time. Using our experimental values of $L_{\text{head}} = 4$ mm, $\eta_{\text{mucus}} = 65$ Pa · s, $A_c = 8.7$ mm², $V_{\text{head}} = 22$ mm³, $E = 500$ Pa, and $h_{\text{mucus}} = 10$ μm, we thus find $\tau_{\text{slip}} \equiv L_{\text{head}}^2 \eta_{\text{mucus}} A_c / V_{\text{head}} E h_{\text{mucus}} \approx 82$ s, which is in reasonable agreement with the empirical mean value of 44 s.

As we show in the main text (Fig. 3 F and G), the tension in the waist is increased during this relaxation/head contraction phase of pulsation. Once the stresses reach a critical threshold, the waist starts to rupture. To estimate the magnitude of these rupture stresses, we again take a linear approach. Taking the deformations of the head to be volume-preserving (because of incompressibility), a radial contraction $\delta R < 0$ induces an axial extension $\delta L_{\text{head}} \approx -2L_{\text{head}} \delta R / R$. This extension implies an axial strain $\varepsilon \approx -2\delta R / R$ and an axial stress $\sigma_{\text{head}} \approx E(-2\delta R / R)$. The latter implies a force on the waist $F_{\text{waist}} \approx (2\pi R) |\delta R| E$ during the relaxation phase of pulsation wave, in agreement with the experimental data (Fig. 3 F and G). Thus, the stress in the waist is $\sigma_{\text{waist}} \approx 2(\pi R^2 / A_{\text{waist}}) E |\delta R| / R$. Because of the differences in cross-sectional areas of head ($A_{\text{head}} = \pi R^2$) and waist region ($A_{\text{waist}} \approx 0.07 A_{\text{head}}$), the longitudinal stress in the waist exceeds the longitudinal stress in the head by a large factor (~ 14). We estimate this critical stress necessary for rupture using experimentally determined parameters only (Table S1) and obtain $\sigma_{\text{waist}} \approx 3,000$ Pa, which is in reasonable agreement with our data from independent traction force measurements.

Effect of Circular Cross-Sections. The cylindrical model assumes that the cross-sectional area of the head and waist are circular. This simplification of the animal's cross-sectional geometry, which in reality is more elliptical than circular (Fig. S1), has only minor effects on the results. Circular cross-sections appear in four aspects of the theoretical description:

- i) The cross-sectional areas affect the stress amplification factor, which is central to our interpretation of the data. To estimate the cross-sectional areas of head and waist, we used ratios of R^2 instead of actual cross-sections. From side-view imaging, we find that the ratios of waist height to head height are on the order of three to four (manual measurement), yielding a cross-section ratio of 11.2–13.9, which is comparable to our estimate of 14.
- ii) Assuming that planarian width and height correlate (as shown in ref. 36), the head extension velocity is unaffected if we use circular instead of elliptical cross-sectional areas.
- iii) During the contraction phase, the head is more circular in cross-section than normal. Thus, while using a circular cross-sectional area leads to an overestimation of the volume, using the elliptical cross-sectional area of an unperturbed worm leads to an underestimation thereof. The head volume enters in the estimation of the contraction time scale as $1/V$. Therefore, the circular cross-section leads to a smaller contraction time than using the elliptical one (82 s versus 109 s). The “true” value lies between these estimates.
- iv) The cross-sectional geometry enters in the Hooke's law estimation of rupture stresses. We assume a certain elongation based on the radial contraction. Using the measured cross-sectional area ratio from the side-view movies of the head and waist (11.2–13.9), we obtain an estimate for the stress in the waist of 2.5–3.1 kPa, which is comparable to our originally reported value (3 kPa) based on a circular cross-section.

In summary, using a circular instead of an elliptical cross-section has a small effect on the contraction time, a negligible effect on the stress estimate, and no effect on the amplification factor and the head extension velocity. Furthermore, it does not affect the qualitative prediction of the model that head and waist extension are anticorrelated.

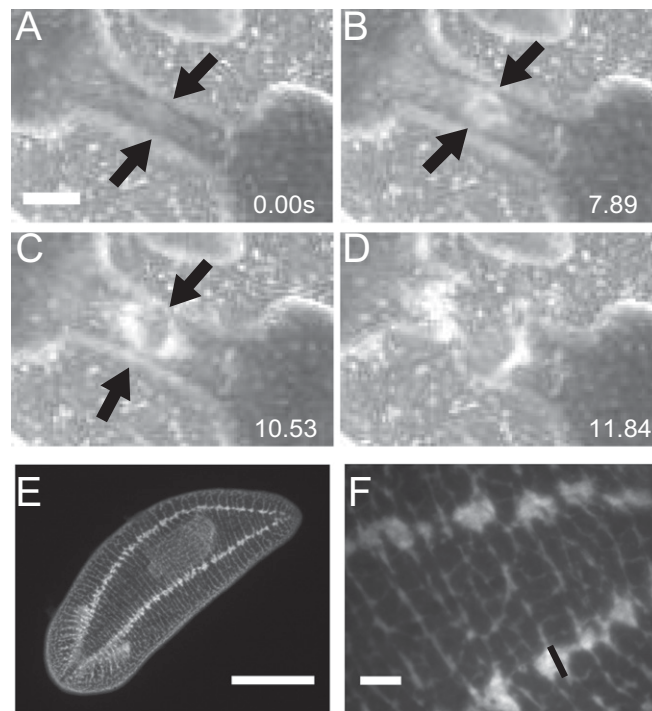
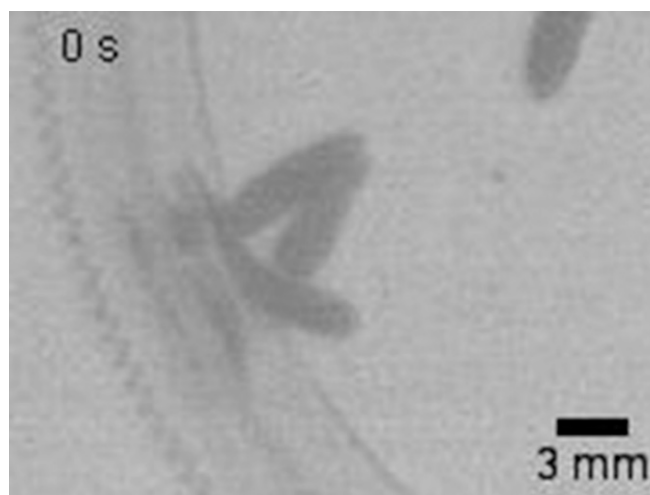


Fig. S7. Nerve cords break last. (A) Worm waist precession; arrows indicate nerve cords at the edge of the worm. (Scale bar: 1 mm.) (B) Beginning of rupture; black arrows indicate nerve cords remaining on the edges of the worm. (C) After initial rupture in the center of the waist has almost completely nucleated outward; black arrows indicate that the nerve cords have not broken, and are some of the last tissue to break. (D) Worm has completely ruptured. (E) Full worm picture of antibody staining against synapsin showing two nerve cords that run along either side of the planarian. (Scale bar: 1 mm.) (F) Zoomed-in picture of E showing nerve cord width is roughly 50 μm. (Scale bar: 100 μm.)

Table S1. Experimental values and estimates that are referenced throughout the text

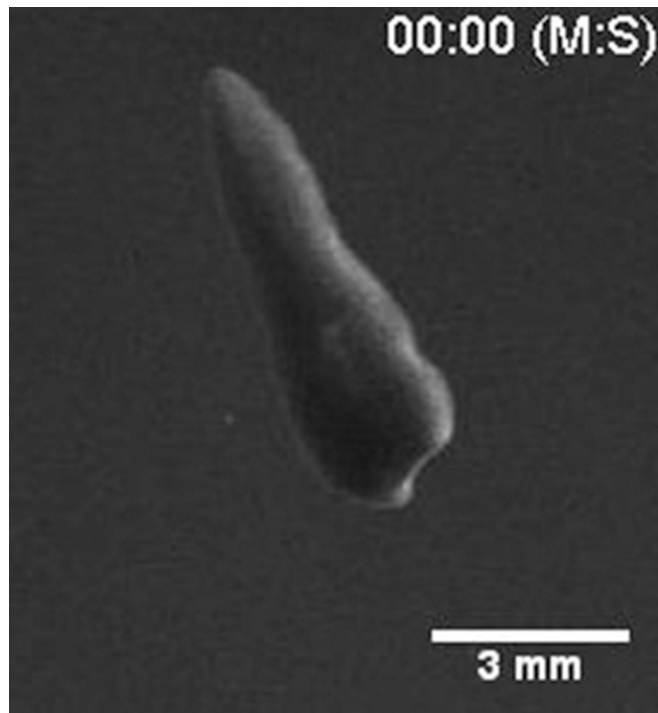
Quantity	Value	Source
Duration of total fission process	17.8 ± 10.1 min ($n = 17$)	Measured duration between initiation of waist formation and rupture
Young's modulus of worm shell (E)	500 Pa	16
Planarian shell thickness (h_{shell})	10 μ m	14
Mucus layer thickness (h_{mucus})	10 μ m	16
Planarian waist radius (R_{Waist})	0.31 ± 0.06 mm ($n = 22$)	Half the measured width of the waist region
Planarian head radius (R)	1.2 ± 0.1 mm ($n = 22$)	Half the measured width of the head piece before pulsation begins
Planarian density (ρ)	1,000 kg/m ³	See description of density measurement in <i>Materials and Methods</i>
Planarian head volume (V_H)	22 ± 11 mm ³ ($n = 22$)	Assuming a cylindrical worm, $V_H = \pi R^2 L$, where R and L are the measured worm head radius and length, respectively
Planarian–substrate contact area ($A_{contact}$)	8.7 ± 3.3 mm ² ($n = 22$)	Measured manually as the area of the worm head profile when imaged from above
Mucus viscosity (η)	65 Pa·s	See Fig. S6B and description of mucus rheology in <i>Materials and Methods</i>
Stress amplification factor (A_{Head}/A_{Waist})	14 ± 3 ($n = 22$)	Assuming both cylindrical head and waist, we have $A_H/A_{Waist} = R^2/(R_{Waist})^2$
Pulse extension velocity (v_{ext})	1.1 ± 0.4 mm/s ($n = 16$)	Using values from logistic fits of extension described in <i>Materials and Methods</i>
Contraction duration (τ_{cont})	44 ± 20 s ($n = 18$)	Measured duration of the linear contraction phase of pulsation
Maximum longitudinal strain (ϵ)	0.43 ± 0.15 ($n = 16$)	Using values from logistic fits of extension described in <i>Materials and Methods</i> , $\epsilon = \Delta L/L_0$
Traction stress on substrate (σ)	100 Pa	Measured from traction force experiments; value reflects the order of magnitude of measured stresses
Radial contraction (δR)	0.27 ± 0.13 mm ($n = 16$)	Difference between maximum and minimum radius in the head during pulsation

This table describes the characteristic values of relevant experimental parameters. The Source column lists either the relevant reference from the literature or the method of calculation and/or measurement. Entries in the Value column that stem from experiment are average values and accompanied by \pm SD.



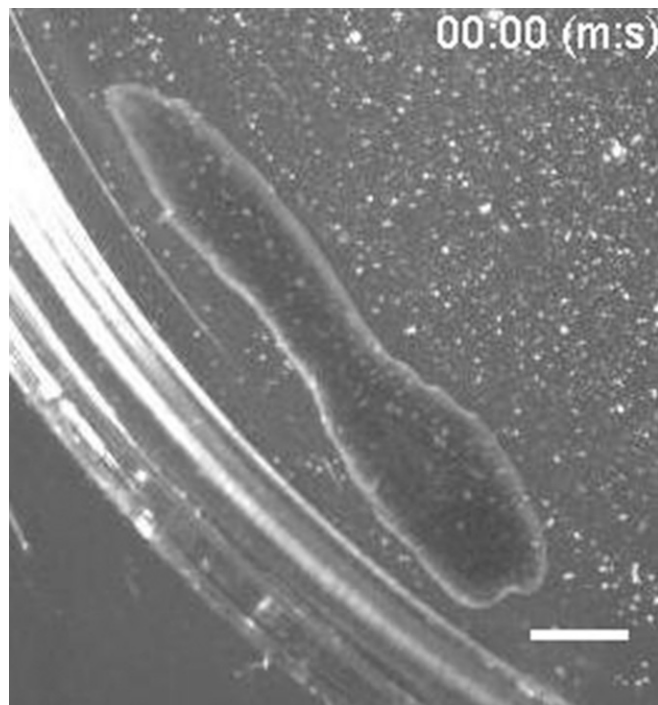
Movie S1. Full fission process from waist formation to pulsation to rupture with a full worm. Movie was recorded at 1 fps and played back at 10 fps. (Scale bar: 3 mm.)

[Movie S1](#)



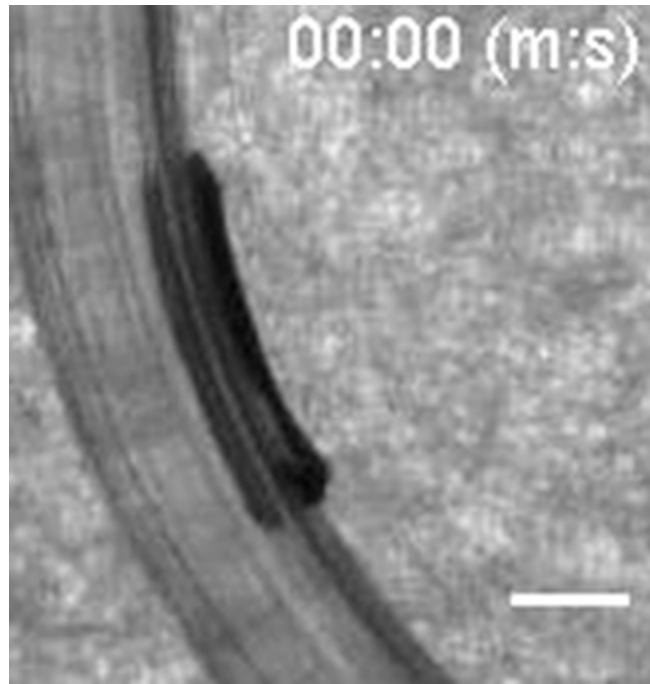
Movie S2. Full fission process from waist formation to pulsation to rupture with a decapitated worm. Movie was recorded at 0.8 fps and played back at 52 fps. (Scale bar: 3 mm.)

[Movie S2](#)



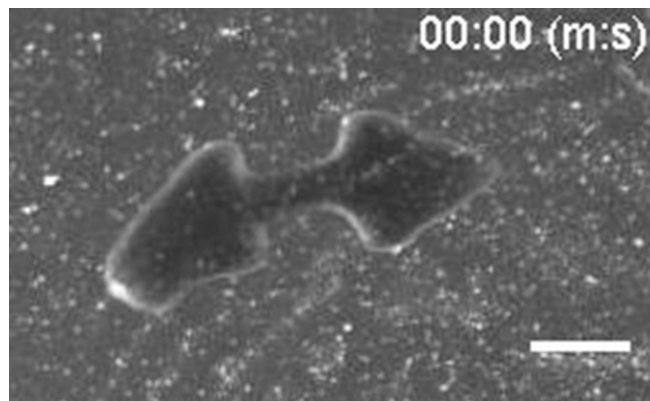
Movie S3. Peristaltic-like contractions in a worm undergoing waist formation. Traveling waves can be seen along the side of the worm accompanying the mass transfer out of the waist. Movie is recorded at 0.8 fps and played back at 10 fps. (Scale bar: 2 mm.)

[Movie S3](#)



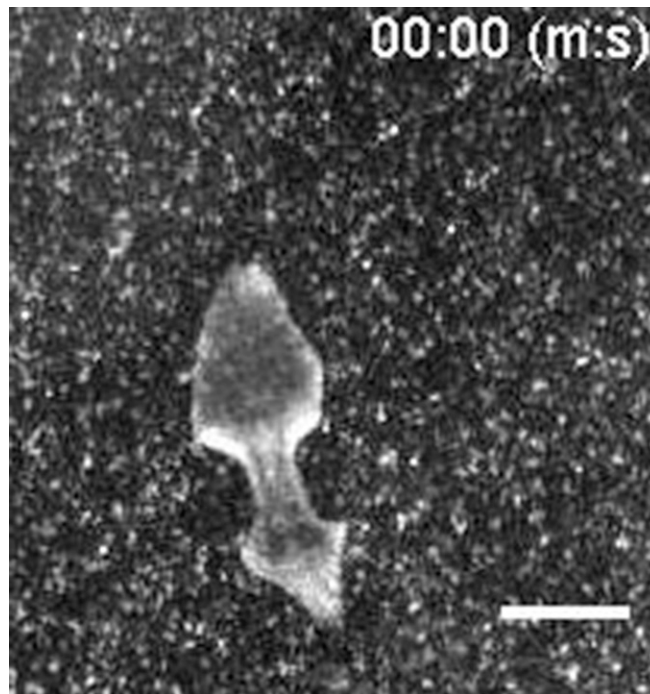
Movie S4. Fission event that occurred against the side of the Petri dish. This shows that the waist is detached from the substrate and the worm lifts its head during the pulsation phase. Vertical oscillations of the waist are also observed. Movie recorded at 5 fps played back at 10 fps. (Scale bar: 2 mm.)

[Movie S4](#)



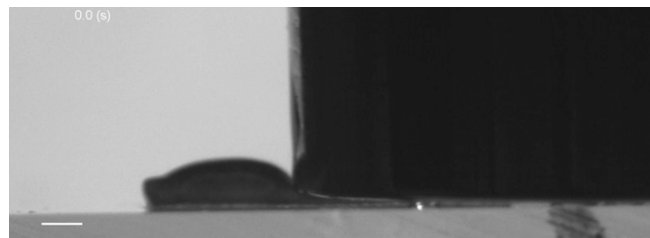
Movie S5. Pulsation phase of the fission process. This movie shows both a head pulse and a tail pulse and the subsequent contractions. One piece undergoes a longitudinal extension while the other piece stays anchored, inducing stress in the waist. Movie recorded at 0.8 fps and played back at 5 fps. (Scale bar: 2 mm.)

[Movie S5](#)



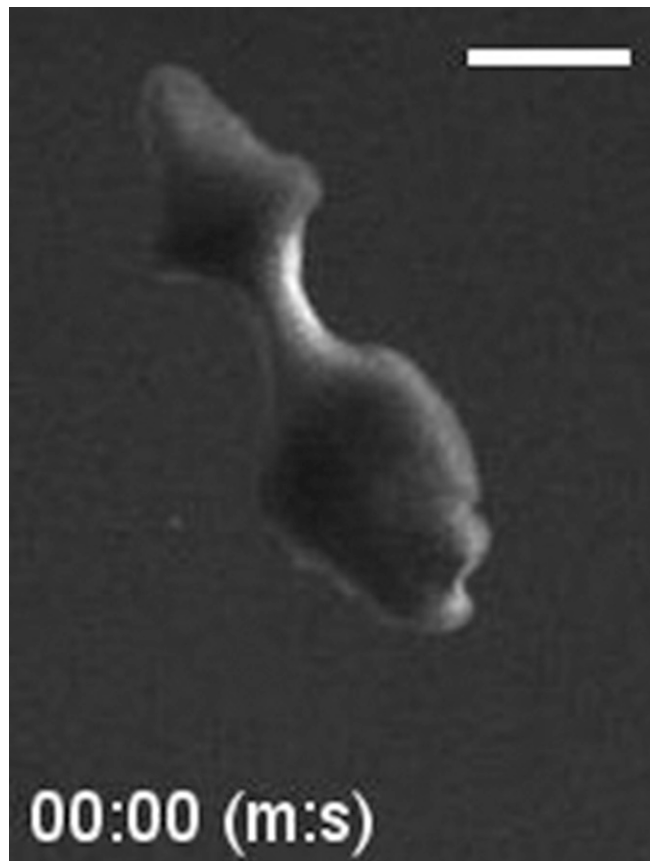
Movie S6. Worm undergoing repeated pulsation before fission. The worm is not able to keep the tail anchored well during the head pulses and is seen to continually slip and move forward. This reduces the potential stress in the waist region. Movie recorded at 0.8 fps and played back at 16 fps. (Scale bar: 2 mm.)

[Movie S6](#)



Movie S7. Side view of worm pinned down with a 5 g weight. During its attempt to escape through fission-like pulsation, the worm lifts its head from the substrate to maximize elongation. Movie recorded at 10 fps and played back at 8 fps. (Scale bar: 2 mm.)

[Movie S7](#)



Movie S8. Successful termination of the fission process marked by a transverse rupture in the waist region. The fracture originates in the center of the waist and propagates outward. Movie recorded at 0.8 fps and played back at 5 fps. (Scale bar: 2 mm.)

[Movie S8](#)